WATER RESOURCES RESEARCH, VOL. 33, NO. 9, PAGES 2049–2063, SEPTEMBER 1997

New piecewise-continuous hydraulic functions for modeling preferential flow in an intermittent-flood-irrigated field

B. P. Mohanty,[1] R. S. Bowman,[2] J. M. H. Hendrickx,[2] and M. T. van Genuchten[1]

Abstract. Modeling water flow in macroporous field soils near saturation has been a major challenge in vadose zone hydrology. Using in situ and laboratory measurements, we developed new piecewise-continuous soil water retention and hydraulic conductivity functions to describe preferential flow in tile drains under a flood-irrigated agricultural field in Las Nutrias, New Mexico. After incorporation into a two-dimensional numerical flow code, CHAIN_2D, the performance of the new piecewise-continuous hydraulic functions was compared with that of the unimodal van Genuchten-Mualem model and with measured tile-flow data at the field site during a number of irrigation events. Model parameters were collected/estimated by site characterization (e.g., soil texture, surface/subsurface saturated/unsaturated soil hydraulic property measurements), as well as by local and regional-scale hydrologic monitoring (including the use of groundwater monitoring wells, piezometers, and different surface-irrigation and subsurface-drainage measurement systems). Comparison of numerical simulation results with the observed tile flow indicated that the new piecewise-continuous hydraulic functions generally predicted preferential flow in the tile drain reasonably well following all irrigation events at the field site. Also, the new bimodal soil water retention and hydraulic conductivity functions performed better than the unimodal van Genuchten–Mualem functions in terms of describing the observed flow regime at the field site.

1. Introduction

Preferential flow under saturated [*Logsdon*, 1995; *Andreini and Steenhuis*, 1990; *Everts and Kanwar*, 1990; *Jardine et al.*, 1989; *White*, 1985; *Beven and Germann*, 1982] as well as unsaturated [*Booltink*, 1993; *Jardine et al.*, 1990; *Wilson et al.*, 1990; *Phillips et al.*, 1989; *Bowman and Rice*, 1986; *White*, 1985; *Beven and Germann*, 1982; *De Vries and Chow*, 1978] conditions through macropores, cracks, and other nonmatrix domains that coexist with the soil matrix domain has been found to be more a rule rather than an exception in structured field soils. Multidomain models are being developed [*Zurmuhl and Durner*, 1996; *Gwo et al.*, 1996; *Hutson and Wagenet*, 1995; *Gerke and van Genuchten*, 1993a, b] to account for this nonideal flow behavior and related solute transport processes in variably saturated soil. Multidomain flow/transport models typically need soil hydraulic conductivity ($K_i(h_i)$, $i = 1, 2, \cdots, n$) and soil water retention ($\theta_i(h_i)$, $i = 1, 2, \cdots, n$) relationships as a function of the pressure head, h_i, for each of the n domains, including terms accounting for the interaction or exchange of water or solutes between the different domains.

Although multidomain approaches are often based on a conceptual analysis of the underlying flow and transport processes [*Jardine et al.*, 1990], most available techniques for measuring soil hydraulic properties (conductivity and retention) can neither distinguish between the different flow domains and their relative contribution to flow [*Luxmoore et al.*, 1990], nor be used to determine the between-domain exchange terms during variably saturated flow, except perhaps when using some type of inverse procedure built upon many simplifying assumptions [*Durner*, 1994]. For purposes of multidomain flow-transport modeling, once the hydraulic functions (K-h and θ-h) are known for one domain (the bulk soil), different θ-h and K-h relationships may be derived for different domains by simply multiplying or dividing the one-domain functions with certain factors. These factors could be selected based upon the statistics of the fractional cross-sectional areas of the domains being considered. For example, *Hutson and Wagenet* [1995] created domain-specific hydraulic functions for their five-domain flow and transport model by applying log-normally distributed scaling factors (having a mean of 1.0 and a standard deviation of 0.25) to the bulk soil $K(h)$ and $\theta(h)$ curves, thus creating an ensemble of five different hydraulic domains of equal area. Their approach in turn resulted in mean $K(h)$ and $\theta(h)$ curves for the five domains similar to those for the single-domain soil. Although this approach of defining characteristic functions for different hydraulic domains may be mathematically appropriate, the task of testing these functions is formidable in view of current experimental limitations.

Some researchers [e.g., *Anderson and Hopmans*, 1994; *Singh et al.*, 1991a, b; *Warner et al.*, 1989; *Edwards et al.*, 1988; *Bouma*, 1981; *Bouma and Dekker*, 1978] attempted to quantify macroporosity, including pore dimensions and pore abundance in different soil horizons, by direct measurement using computer tomography, AUTOCAD, image analysis, resin impregnation, or some other method. These studies were aimed at modeling macropore flow on the basis of the number and geometry of pores, as was suggested by *Edwards et al.* [1979]. On the other hand, *Ela et al.* [1992] suggested that knowledge of the number and size of visible macropores by itself may be insufficient to model water infiltration through macropores. A more practical

[1]U.S. Salinity Laboratory, USDA-ARS, Riverside, California.
[2]New Mexico Institute of Mining and Technology, Socorro.

Paper number 97WR01701.
0043-1397/97/97WR-01701$09.00

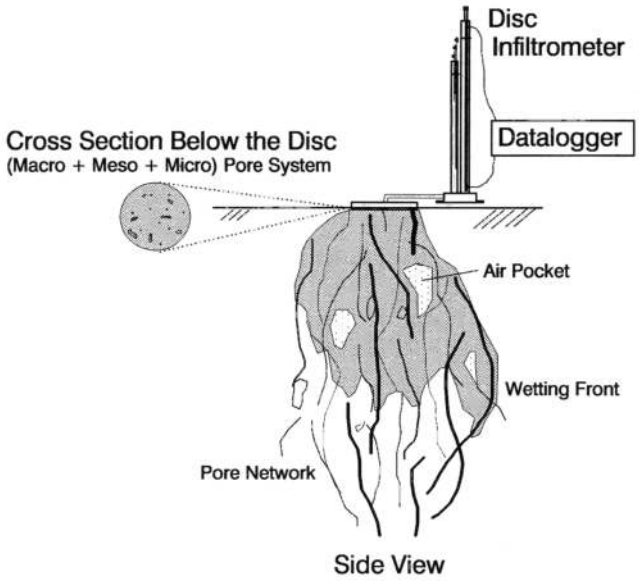

Figure 1. A close view of the pore system in the bulk soil under disc infiltrometer during in situ hydraulic conductivity measurement. $K(h)$ near saturation is the composite value for the bulk soil including micropores, mesopores, macropores, and cracks. Thickness of irregular lines indicates pore size.

indirect approach was proposed by *Watson and Luxmoore* [1986] and later advocated also by *Wilson et al.* [1992] and *Mohanty et al.* [1996], among others. They used the difference of the hydraulic conductivity measured at 0-cm and 3-cm soil water tensions using disc infiltrometers to define the macropore conductivity and using Poiseuille's equation to estimate the effective macroporosity of certain (>1-mm) diameter pores as recommended by *Luxmoore* [1981]. Although this method in essence is a lumped approach that cannot yield the interaction/exchange terms in multidomain models, the method does permit better measurement of the hydraulic properties of soils near saturation.

The accuracy of soil water content measurements is generally limited by the error of the measurement method. Unfortunately, it is experimentally very difficult to measure the retention characteristics of a soil accurately and reproducibly at very low suctions. It is further questionable whether retention curves can properly represent the pore-size distribution of a porous medium at high saturation where the nonwetting phase (air) is not continuous [*Corey*, 1992]. This means that hydraulic conductivities predicted from retention data are inherently inaccurate when approaching saturation, even if one assumes that the predictive conductivity model itself is error-free and applies to all pore sizes. As a consequence, hydraulic conductivity estimation from soil water retention functions that represent a certain pore space near saturation (e.g., h less than 1 cm) are inherently unreliable, regardless of whether unimodal or multimodal functions are used. This is generally also the case when the parameter n in van Genuchten's retention equation ($m = 1 - 1/n$) is close to unity [*Durner*, 1994].

Disk infiltrometry methods involving ponded and tension infiltrometers [e.g., *Ankeny et al.*, 1988; *Prieksat et al.*, 1992] are now increasingly used for measuring hydraulic conductivity in situ at low soil water tensions (i.e., close to saturation). One advantage of these methods is that negative soil water pressures at the soil-infiltrometer interface can be maintained very close to zero and be decreased in small increments to get precise K-h functions near saturation [*Jarvis and Messing*, 1995; *Messing and Jarvis*, 1993; *Clothier and Smettem*, 1990]. Using this macroscopic approach, one important assumption is that the soil water pressure head across the disc surface will remain uniform and thus in equilibrium with the soil medium for all "conducting" pore sizes and flow domains, including the larger macropores. Hence the soil water pressure head maintained in the infiltrometer represents the weighted average for all "conducting" flow domains that coexist below the disc (Figure 1). Since this method assumes a uniform head (i.e., water maintained at a certain positive or negative soil water pressure) or uniform flux (i.e., water application rate) across the soil surface, flooding/ponded irrigation (as in our field site) could provide an attractive condition to test the performance of alternative new hydraulic conductivity functions at and near saturation. Note, however, that no bypass flow, as that which may occur under nonequilibrium conditions through macropores, is involved in this approach (i.e., all small pores at any given depth have to be filled before the water is transported only or mainly through the large pores).

The goal of this study hence is to develop physically realistic, yet practical (based on actual measurements) soil water retention and hydraulic conductivity functions for describing subsurface water flow and related preferential solute transport processes in a macroporous agricultural field under irrigation. Main focus is on the development and testing of new piecewise-continuous hydraulic functions based on in situ and laboratory measurements of the soil water retention and hydraulic conductivity using small increments in h. The new functions will be used to predict observed preferential water flow into tile drains following several irrigation events at a field site in Las Nutrias, New Mexico. Furthermore, performance of the new bimodal hydraulic functions will be compared with the traditional unimodal van Genuchten-Mualem model. A follow-up paper will address solute transport during preferential flow at the same field site.

2. Field Site and Hydrology Monitoring

Our experimental field site is located on a 24-ha commercial agricultural farm, situated on an alluvial flood plain of the Rio Grande, near Las Nutrias, New Mexico. The basin lies within the Rio Grande rift, a series of north-south trending half grabens oriented parallel to the course of the Rio Grande. The climate is arid to semiarid and has a wide range of temperatures and rainfall. The parent material for the entire valley is alluvium. Plate 1 shows the major soil classes across the 6-ha center bench of the field, including our study section. In general, the field site consisted of silty clay loam sediments with moderate to poor drainage properties, underlain by fine sands, and with no impeding strata to a depth of about 7 m [*Natural Resource Conservation Service (NRCS)*, 1992]. Surface horizons, however, contained visible root channels, worm holes, and cracks, thereby composing a complex network of preferential flow paths. The field was relatively flat and divided into three benches, namely, east (240 × 270 m), center (240 × 270 m; Figure 2), and west (420 × 270 m), separated by two berms. To sustain agricultural productivity, the field site was equipped with surface irrigation and subsurface (tile) drainage systems to reduce salinity in the crop-root zone. The subsurface tile drainage system consisted of four lateral drain lines installed approximately at a depth of 1.2 m. The tile drains

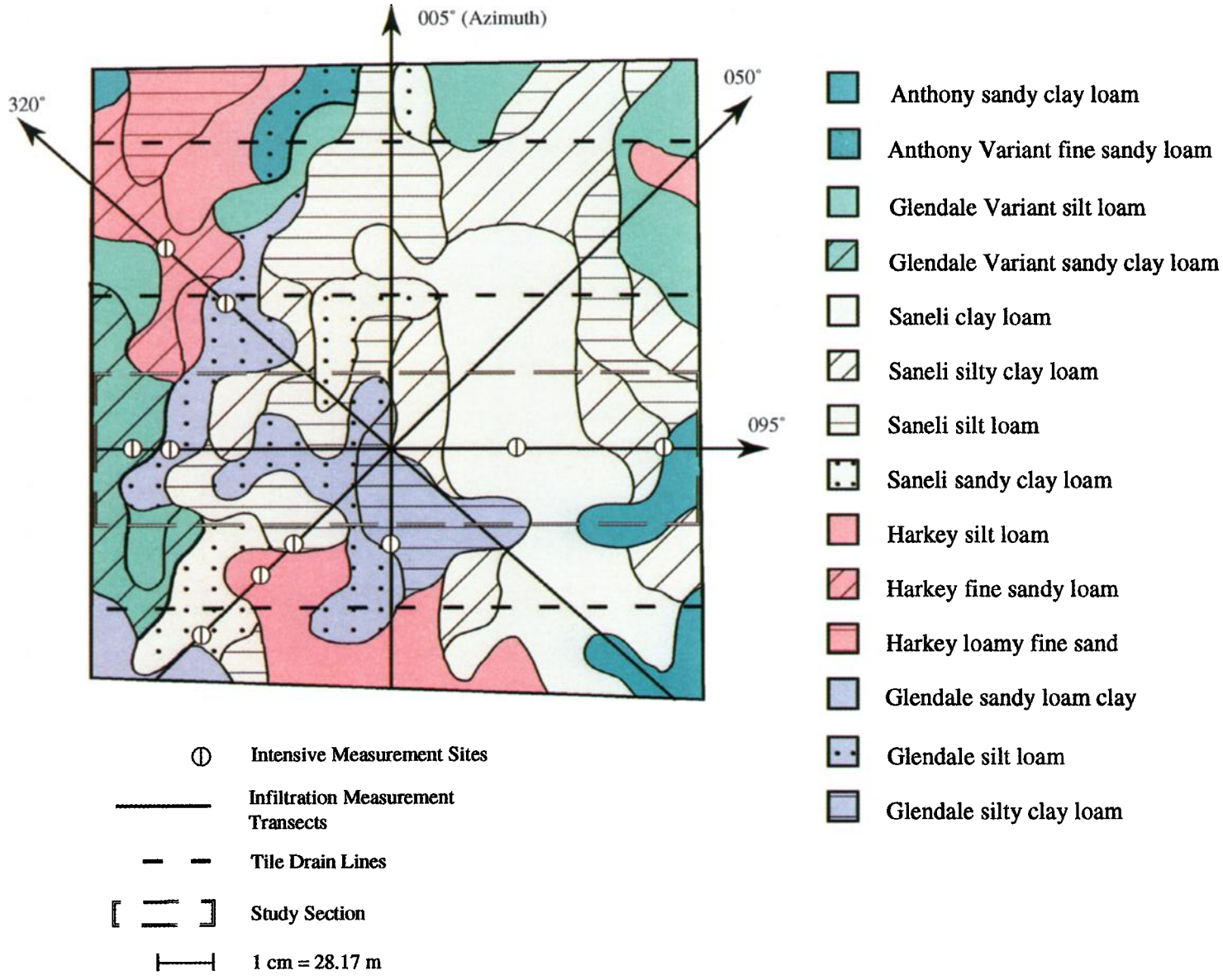

Plate 1. Soil series map of the center bench at the Las Nutrias field site, in New Mexico. Study section contains four major soil series that in turn have different soil textural classes.

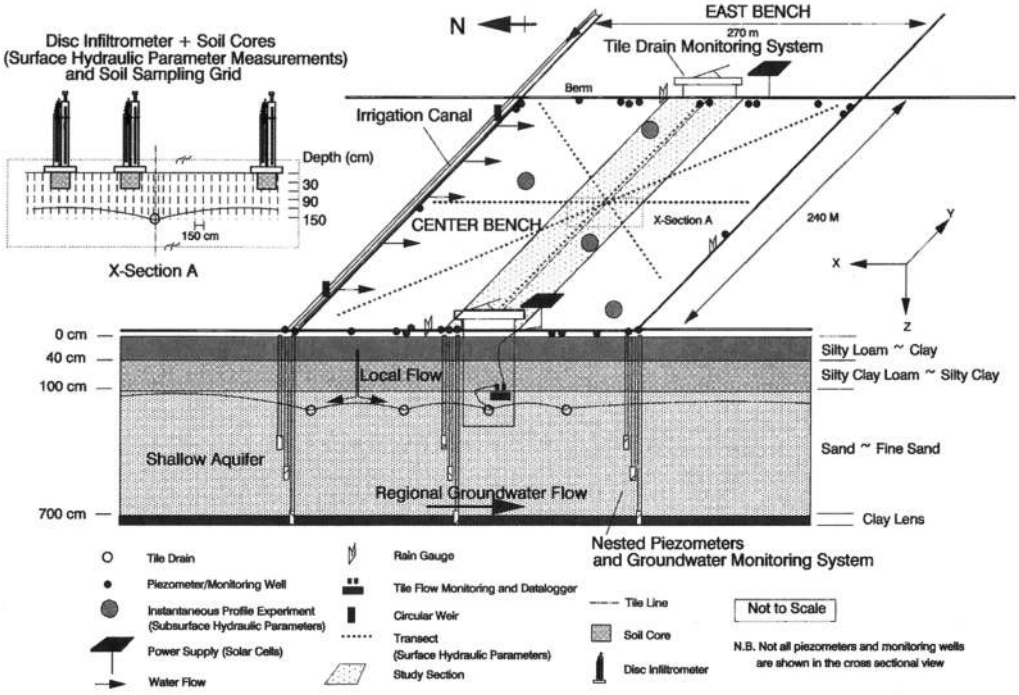

Figure 2. Three-dimensional view of the field site including important hydrology monitoring facilities and the locations of surface and subsurface site characterization studies.

connected to a main drain line leading to an off-site open-channel drain on the west. Irrigation return flows draining from the field, as well as periodic build up of shallow groundwater flowing in from off-site areas, were collected by this system. A southern section of the center bench drainage system was isolated by installing two manholes along a single drain line at the east (up) and the west (down) ends of the bench. The manholes allowed regular sampling of water quantity and quality entering and leaving that (study) section of the drain line. The manholes were equipped with Signet® flow measurement systems including data loggers for monitoring flow rates at 5-min intervals. We used this isolated section of the center bench for collecting soil hydraulic parameters and for monitoring flow in the vadose zone. Horizontal and vertical pressure gradients at different (2-, 5-, and 7-m) depths in the underlying aquifer were determined regularly using piezometers and observation wells along the periphery of the field site. For this purpose, eight nested piezometers at 2-, 5-, and 7-m depths and 33 monitoring wells at 2-m depth (Figure 2) were installed around the field. Three rain gauges were located on the center bench to monitor the average precipitation input of individual rainfall events. A concrete-lined canal on the north side of the field supplied irrigation water to all three benches through a number of control gates using flood-irrigation practice. Irrigation water moved from the north end of the field to the south end in about 4–7 hours and remained ponded in the field for several hours with simultaneous infiltration. After the required amount of water was delivered to the field, irrigation supply was cut off, thus allowing continued variably saturated flow and redistribution within the soil profile. A 25-cm diameter circular weir of the type developed by *Samani* [1993] was used in the irrigation canal to measure water input to the center bench during each irrigation event. The farmer scheduled the water input events to different benches depending on the consumptive needs of different crops at different growth stages. Table 1 shows the irrigation dates and amounts including the bench sequence during 1994 and 1995. In general, all three benches received water on the same day, although irrigation in three benches was spread occasionally over 2-day periods. Table 2 shows the crop rotation for 1994/1995.

3. Site Characterization

Surface infiltration is by far one of the most important variables to determine the behavior of any field-scale flow and transport process. Disc infiltrometers including ponded- and

Table 1. Irrigation Application Dates and Volumes Applied to the Center Bench

Date	Total Elapsed Time, Hours	Total Volume, L	Total Depth, mm	Bench Sequence
June 8, 1994	4.5	4.14E+06	61.22	E-C-W
June 27, 1994	7.0	4.56E+06	67.43	E-C-W
Aug. 8, 1994	6.0	5.10E+06	75.41	E-C-W
Sept. 28, 1994	7.5	5.88E+06	86.93	W-C-E
April 10, 1995	6.0	6.47E+06	95.76	E-W-C
April 26, 1995	6.5	5.37E+06	79.48	E-W-C
May 15, 1995	6.0	6.77E+06	100.09	E-W-C
June 5, 1995	6.0	6.17E+06	91.23	E-C-W
June 19, 1995	7.5	6.18E+06	91.46	E-C-W
July 10, 1995	7.0	6.84E+06	101.26	E-C-W
July 28, 1995	7.4	6.65E+06	98.41	W-C-E
Aug. 8, 1995	4.8	4.98E+06	73.62	E-W-C
Sept. 7, 1995	4.2	4.08E+06	60.37	W-C-E
Sept. 26, 1995	4.5	5.07E+06	75.03	W-C-E
Oct. 23, 1995	7.2	7.78E+06	115.03	W-C-E

Bench sequence indicates the order of water application during a particular irrigation event. E, east bench; C, center bench; W, west bench.

tension-infiltrometers were used to measure the K-h relationship in the near-saturation pressure head range (i.e., low soil water tension range). To incorporate field-scale variability in hydraulic properties resulting from different soil types and pore-size distribution across the field, in situ hydraulic conductivity measurements at 104 selected sites along four transects (as shown in Plate 1) were made. Since the flow regime in the vadose zone and in the shallow groundwater aquifer at the center of the study section was two-dimensional with flow lines converging to the tile line, we implemented a more rigorous parameter estimation effort across the north-south transect orthogonal to the tile line, which was oriented in an east-west direction. On the basis of the tile-drainage design, the particular tile supposedly served a 75-m-wide and 240-m-long section of the center bench. To better define the subsurface flow field of the section, we selected 61 sites along the north-south transect located symmetrically across the tile line. Sequential grid spacings of 2 × 0.5 m, 1 × 1 m, 25 × 1.5 m, 1 × 12 m, and 1 × 15 m were used on both the north and south sides of the tile line. Each of the remaining three transects contained 15 measurement locations. All hydraulic property measurements along the east-west transect were taken directly above the drain line with a regular spacing of 15 m. The measurements along the diagonal transects were made at 18-m intervals. All measurements were later used for estimating field-average (⟨ ⟩) hydraulic properties using simple (geometric or arithmetic) averaging schemes. Surface infiltration measurements at 0-, 30-, 60-, and 150-mm soil water tensions were made at these sites in the summer of 1994, using experimental procedures as described in a similar previous study by *Mohanty et al.* [1994, 1996]. To minimize any site disturbance, the water-supply tower of the tension infiltrometer was refilled during the experiment using the procedure of *Ankeny* [1992]. In addition to measurements at the aforementioned soil water tensions, 10 sites across the center bench representing different soil types were selected for conducting infiltration measurements between 0- to 30-mm soil water tensions at 2- to ~5-mm tension increments. *Ankeny* [1992] cautioned that infiltration for tensions below 10 mm should be interpreted carefully because of the possible inaccuracies in the applied tension owing to bubbling. As such, we interpreted the infiltration rate in this narrow range of tensions only in a qualitative manner so as to reveal relative trends near saturation. The data were used to develop new piecewise-continuous hydraulic conductivity functions whose fitting parameters could be further adjusted during model calibration. For the above intensive infiltrometer measurements, we used thin layers (1 ~ 2 mm) of contact sand to minimize any interfacial effect of the sand on the infiltration rate close to saturation as reported by *Everts and Kanwar* [1993]. The actual tensions at the soil surface as reported here were estimated by assuming unit-gradient water flow through the sand layer and by reducing the tension at the base of the infiltrometer by the average sand depth.

Following the surface infiltration measurements, 5-cm-diameter and 5-cm-long undisturbed soil cores were collected directly below the disc from the same 10 sites representing different soil series and textures across the field. The soil cores were subsequently used for measuring the water retention and hydraulic conductivity for a wider range (0 to 1700 mm) of soil water tensions. The laboratory method of *Richards* [1965] and the multistep outflow approach of *Gardner* [1956] were used for measuring soil water retention and hydraulic conductivity functions, respectively. Similar to our approach in the field, we were mostly interested in relative trends rather than absolute values of the retention data near saturation. While the actual numbers may be imprecise, they could be adjusted by subsequent calibration of selected parameters in the new piecewise-continuous retention function so as to better represent the flow scenario at the field site. For this purpose the in situ and laboratory experiments were carried out as carefully as possible using very small increments in the tension near saturation.

Table 2. Crop Rotation Schedule for the Center Bench

Crop	Planting Date	Harvest Date(s)
Winter wheat	Oct. 10, 1993	not harvested
Sorghum-Sudan cross	May 13, 1994	July 19, 1994
Alfalfa	Sept. 25, 1994	May 29, 1995
		June 2, 1995
		July 5, 1995
		Aug. 6, 1995
		Sept. 6, 1995
		Oct. 15, 1995

For subsurface horizons, water retention and hydraulic conductivity properties at four representative sites in the field (Figure 2) were measured using the instantaneous profile (IP) method [*Watson*, 1966]. Particle size estimates to a depth of 1.5 m at 200 sites on a regular square grid across the center bench were used to locate the representative profiles on the basis of the occurrence of similar textural layering in different horizons. Since the groundwater table at the field site was approximately 40 ~ 50 cm lower during spring than in the summer, we conducted a 3-week long instantaneous profile experiment during the spring of 1995. Each IP experimental plot was equipped with a neutron probe (at the center) and 18 tensiometers installed at different depths up to a depth of 1.2 m. Soil water contents and pressure heads at different depths were measured at 30-min intervals at the beginning of the experiment; frequency was decreased gradually to several hours/days on the basis of the rates of change in the observed data. The data were analyzed to define the soil water retention and hydraulic conductivity functions at different depths (horizons) across the soil profile for subsequent use as input parameters for the numerical flow simulations.

4. Initial and Time-Dependent Boundary Conditions at the Field Site

In late February 1994 soil water content measurements were made on a parallel transect, 1 m off the original north-south transect used for the surface infiltration measurements (Figure 2). The same transect was followed for defining the initial (water table) conditions across the two-dimensional finite element grid for numerical simulation of the flow field at the field site. Soil samples were collected at 30-cm increments up to a depth of 120 cm using Veihmeyer® soil sampling tubes. These samples were later used for gravimetric measurements of the soil water content in the laboratory. Because of uncertainity about the possible effects of freezing at the field site during the winter of 1994/1995, we repeated the soil water content measurements along the same transect in February 1995. The spring soil water content data were later used to define initial conditions for the flow simulations. These initial conditions were thought to be appropriate for estimating and simulating surface-contributed flow into the subsurface tile drains since

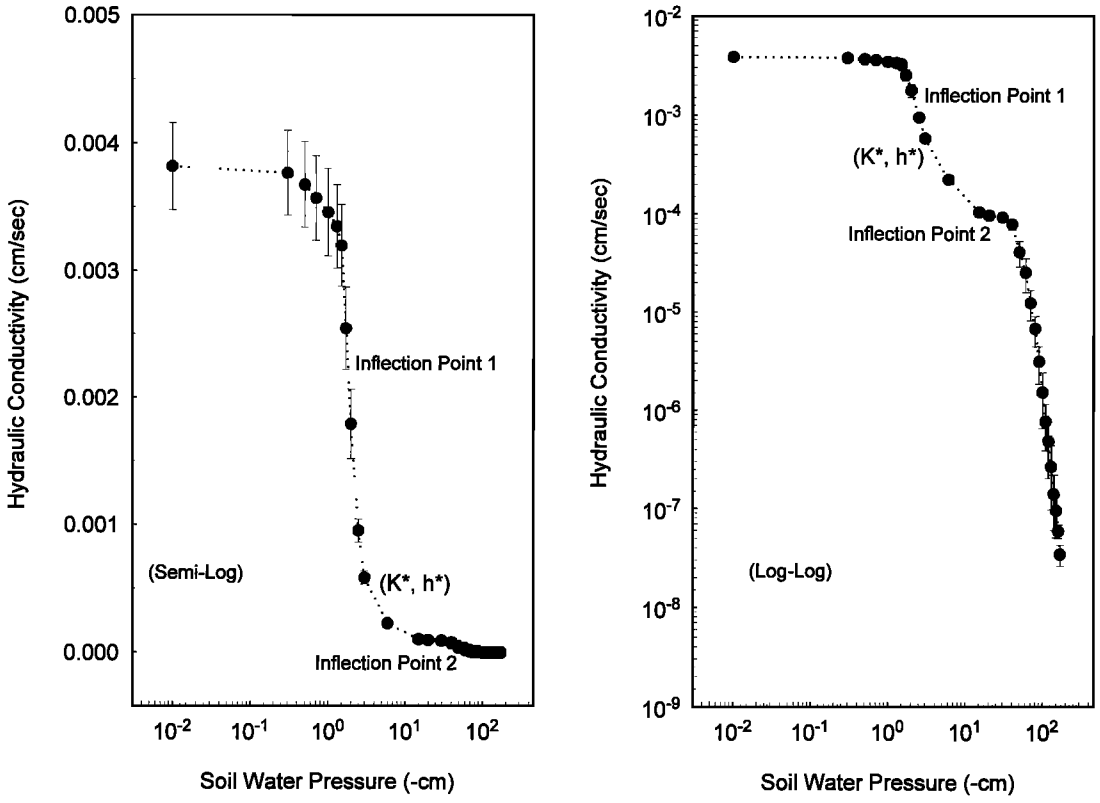

Figure 3. Error bar (geometric mean and standard error) plots of the ⟨field-averaged⟩ soil hydraulic conductivity (K-h) function for the surface horizon by superimposing the in situ and laboratory measurements: (a) semilog plot and (b) log-log plot. Inflection points were found between 1.5 and 3 cm (1), and between 3 cm and 30 cm (2). Inflection point 1 near saturation indicates that the flow-governing process changes from non–capillary dominated to capillary dominated.

the regional groundwater flow contribution was relatively small immediately after the spring irrigation events. In addition to intermittent irrigation and rainfall events, preestablished empirical relationships for the geographical region and crops [*Mapel et al.*, 1985] were used for calculating time-dependent evapotranspiration rates from the top soil layers near the soil-atmosphere boundary.

In addition to the soil water content measurements along the transect, the observation wells and piezometers along the boundary of the field were monitored once a month to estimate the water table head and its gradient associated with regional groundwater flow below the field site. Water table heights were interpolated to define time-dependent hydrologic boundary conditions for the two-dimensional (or pseudo three-dimensional) numerical flow domain. Slug tests were conducted in the piezometers to define the hydraulic conductivity of the aquifer at deeper depths. A thick clay lens at a depth of 7 m below our field site [*NRCS*, 1992] served as the lower no-flow boundary for the numerical simulations. We believe that the assumption of an impermeable boundary is reasonable since this study focused on short-term preferential flow phenomena in the tile drains resulting from surface irrigation events.

5. Soil Water Retention and Hydraulic Conductivity Functions

The hydraulic conductivity data obtained with the ponded infiltrometer, tension infiltrometer, and laboratory outflow experiments were superimposed across the tension range of 0 to 1700 mm for all measurement sites. Considering the lack of any single instrument for measuring the hydraulic conductivity across the entire soil water tension range from wet to dry, the superimposition approach of *Clothier and Smettem* [1990] appears to be very practical for characterizing the hydraulic conductivity function of any field soil exhibiting preferential flow near saturation. However, we emphasize that the resulting hydraulic conductivity function is still based on the use of average soil water tensions across the entire pore-size range for the soils under investigation. In other words, the hydraulic conductivity function represents the bulk soil rather than specific flow domains as required in the multiporosity modeling approach. While the latter approach may be more suitable when different pore groups can be quantified, for example, in a controlled column experiment, the lumped method seems more practical for addressing large-scale in situ flow problems. Note that the disc (infiltrometer) surface area (182.4 cm^2) is assumed to encompass the representative elementary volume (REV) of soil for all possible pore (flow) domains at the field site. Figure 3 shows semilog and log-log plots of the field-average K-h curve based on 82 measurements across the study section of the center bench. Interestingly, the ⟨field-averaged⟩ hydraulic conductivity curve for the surface soil showed three turning (or two inflection) points within the measured tension range, that is, at approximately 15, 30, and 300 mm. The sharp changes in K across the inflection point between 15 and 30 mm suggests the presence of relatively fast (preferential) flow phe-

nomena near saturation. When the K-h functions were plotted for the individual measurement sites (not shown here), we encountered similar inflection points although their positions on the curves varied somewhat from site to site. Also, we found that the standard errors of the hydraulic conductivity in the tension range of 0 (K_0) to 20 mm (K_{20}) were much larger in comparison with standard errors in K_h at higher tensions (h) (Figure 3).

Several studies [*Jarvis and Messing*, 1995; *van Genuchten*, 1994; *Wilson et al.*, 1992; *Campbell and Shiozawa*, 1992; *van Genuchten et al.*, 1991; *Clothier and Smettem*, 1990; *Seyfried and Rao*, 1987] have inferred that because of its large variability, the saturated hydraulic conductivity (K_s or K_0 as per our convention) is not a good physical parameter for fitting or scaling hydraulic functions of field soils. For example, *Booltink et al.* [1991] found that K_0 varied from 10 to 5500 cm/day and that these two values generated two distinctly different K-h functions near saturation. In spite of these findings, K_0 is still popularly used as a matching point in most hydrologic studies since this parameter can be more easily measured. This use of K_0 can lead to extreme underpredictions or overpredictions of related hydraulic parameters (e.g., α in Gardners' model or α and n in the van Genuchten–Mualem model), thereby also affecting the accuracy of numerical simulations using those data. By using tension infiltrometers for measuring K_h at different soil water tensions (h) in situ, we explored other more appropriate K_h values as possible matching points for the hydraulic conductivity functions. Such an approach had been advocated by, for example, *Campbell and Shiozawa* [1992] and *Luckner et al.* [1989] as an alternative to the traditional approach of fitting K at zero tension. *Clothier and White* [1981] and *Smettem and Collis-George* [1985] found somewhat similar approaches useful for determining ponding time and for infiltration modeling, respectively, although the exact position of the matching point may remain somewhat arbitrary.

Similar to the Figure 3, Figure 4 shows measured soil water contents (θ-h) across the soil water tension range. Although the soil water content data near saturation are not very precise, one may still notice a very small but conceptually important increase in θ in the tension range of 30 to 0 mm. This result confirms similar findings by *Wilson et al.*, [1992] and *Germann and Beven* [1981]. Moreover, our result qualitatively supports *Hoogmoed and Bouma* [1980], who claimed that lateral absorption from macropores into the soil matrix during bypass flow is in the order of only a few percent. Figure 4 (field-averaged soil water retention) and Figure 3 (field-averaged hydraulic conductivity) over the same (30- to 0-mm) tension range, indicate that while the hydraulic conductivity showed a sevenfold (or 550%) increase, water retention increased only very little. This is consistent with similar findings by R. W. Skaggs (personal communication, 1995), *Clothier and Smettem* [1990] and *Seyfried and Rao* [1987]. We believe that the soil water retention function of the macroporous soil combines several features of both the rigid soil matrix and swell-shrink macropores as was suggested by *Klute* [1986]. *Mohanty et al.* [1996], *Booltink and Bouma* [1993], and *Watson and Luxmoore* [1986] found for similar field studies that approximately 80–90% of total infiltration occurs close to saturation between tensions of 0 and 30 mm. All of the above findings seem to indicate that in this narrow soil water tension range, water is mostly gravity driven and partially mobile and that this water can increase the flux many fold. At the same time, total water retained in the bulk soil appears to remain relatively constant in this range. The

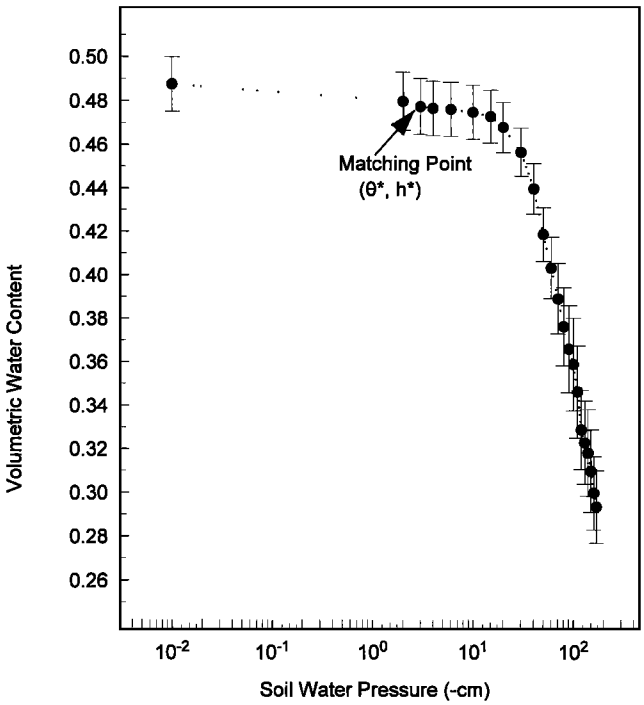

Figure 4. Error bar (arithmetic mean and standard error) plot of the ⟨field-averaged⟩ soil water retention (θ-h) function for the surface horizon measured in the laboratory. Turning point at 30 cm indicates the bubbling pressure.

very small increase from $(\theta_h)^*$ to (θ_0) (in Figure 4) may be only an experimental artifact, which, if true, suggests that water content at this tension range could be equated to $(\theta_h)^*$ for all practical purposes, even for macroporous field soils. However, because only one data point between $(\theta_h)^*$ and (θ_0) was available, a reasonable statistical analysis could not be performed to verify our claim. This situation could be approximated numerically by imposing a slightly higher value at 0 tension than at h^* and using linear interpolation between h^* and 0.

Closed-form van Genuchten–Mualem type models [*van Genuchten*, 1980] for the soil water retention and hydraulic conductivity have been quite successful in describing variably saturated flow as long as the soil has a relatively unimodal pore size distribution [e.g., *van Genuchten and Nielsen*, 1985]. When the soil has a multimodal pore-size distribution, these models become inaccurate close to saturation [*Durner*, 1994, and references therein]. One reason for this failure is a disruption in the otherwise smooth pore-size distribution of a macroporous soil at or near the larger pores. Also, gravity flow through the larger pores during near-saturated conditions will dominate capillary flow which was the basis of Mualem's model. More recently, several researchers [*Mallants et al.*, 1995; *Durner*, 1994; *Othmer et al.*, 1991; *Peters and Klavetter*, 1988] have achieved some success in modeling the hydraulic properties of bimodal or multimodal soils using sums of a number of van Genuchten–Mualem type functions. They found that these multimodal hydraulic functions did perform better than unimodal hydraulic functions at intermediate soil water suctions (pF 1 to 5). However, the sum functions generally did a better job only in optimizing either the retention or the hydraulic conductivity function near saturation, but not both [*Durner*, 1994]. Another group of researchers [*Jarvis and Messing*, 1995; *Messing and Jarvis*, 1993; *Wilson et al.*, 1992] used a number of

piecewise-continuous Russo-Gardner type [*Russo*, 1988] functions, joined at different junction points, for describing the retention and hydraulic conductivity of different pore groups. Although these exponential models (for the hydraulic conductivity) could somewhat better fit the actual data close to saturation [*Messing and Jarvis*, 1993], they became less accurate at midrange soil water suctions. These findings for sum and junction type functions suggest that the soil water retention and hydraulic conductivity functions of multimodal field pore systems should be treated separately [*Logsdon*, 1995]. Moreover, both the sum and junction approaches have their related mathematical and numerical advantages and limitations [*Rossi and Nimmo*, 1994]. Thus, for field soils having multimodal pore size distributions, it may be more appropriate to invoke a hybrid sum-junction approach involving two or more piecewise-continuous functions based on the dominant physical (gravity, capillarity, or adsorption) forces associated with different conducting pore regions across the soil water tension range.

The above findings by different researchers, as well as our own measurements, suggest that the van Genuchten retention function in conjunction with Mualem's hydraulic conductivity function should be used only with care in a small but critical tension range near saturation for macroporous field soils. In other words, the van Genuchten–Mualem models should be used only for tensions greater than h^* (e.g., 3 cm for our case study) when capillary flow dominates, in conjunction with other more appropriate models for the soil water retention and especially the hydraulic conductivity curve for tensions less than h^* when gravity flow dominates. The threshold tension h^* may well change from soil to soil. Nonlinear optimization [e.g., *Wilson et al.*, 1992] could be used to filter out the inflection points in the soil water retention and hydraulic conductivity curves and hence to distinguish between the different flow regions. In this study, however, visual examination of these functions was assumed to be sufficient, and h^*_θ (for the soil water retention function) was approximated with h^*_K (for the hydraulic conductivity function). To avoid confusion when defining our new hydraulic functions at 0 and h^* tensions, we will henceforward use K and θ with the related tension values as subscripts.

Hybrid sum-junction hydraulic functions (1)–(5) follow. For a multimodal pore-size distribution the new soil water retention and hydraulic conductivity functions can be written as

$$\theta(h) = \sum_c w_c\theta_c(h) = \sum_c w_c\left[\theta_{r,c} + \frac{\theta_{s,c} - \theta_{r,c}}{[1 + (\alpha_c h)^{n_c}]^{m_c}}\right] \qquad (1)$$

$$h \le h^*_\theta$$

$$\theta = \theta_{s(c=1)} \qquad h > h^*_\theta \qquad (2)$$

$$K(h) = \sum_c w_c K_c(h)$$

$$= \sum_c w_c \frac{(1 - (\alpha_c h)^{n_c-1}[1 + (\alpha_c h)^{n_c}]^{-m_c})^2}{[1 + (\alpha_c h)^{n_c}]^{m_c/2}} \qquad (3)$$

$$(m_c = 1 - 1/n_c) \qquad h \le h^*_K$$

$$K_{nc}(h) = K^* + K^*[\exp^{(h-h^*)\delta} - 1] \qquad h^*_K < h \le 0 \qquad (4)$$

$$K_{nc}(h) = K^* + K^*[\exp^{(-h^*)\delta} - 1] \qquad h > 0 \qquad (5)$$

where

K_c the hydraulic conductivity for capillary dominated flow domain c [$L\ T^{-1}$];

K_{nc} the hydraulic conductivity for non–capillary dominated flow domain nc [$L\ T^{-1}$];

$\theta_{s,c}$ the saturated water content for capillary dominated flow domain c [$L^3\ L^{-3}$];

$\theta_{r,c}$ the residual water content for capillary dominated flow domain c [$L^3\ L^{-3}$];

h the equilibrium soil water pressure head for bulk soil (across all flow domains) [L];

$h^*_K \approx h^*_\theta = h^*$ the critical or break-point soil water pressure head where flow changes from capillary dominated to non–capillary dominated flow or vice versa [L];

K^* the hydraulic conductivity corresponding to h^* [$L\ T^{-1}$];

δ a fitting parameter representing effective macroporosity or other structural features contributing to non–capillary dominated flow [L^{-1}];

α_c, n_c the van Genuchten fitting parameters [*van Genuchten*, 1980] for the capillary dominated flow domain c [L^{-1}, –],

c the number of capillary dominated flow domains where for $c = 1$ the sum type multimodal van Genuchten–Mualem hydraulic functions (equations (1) and (3)) reduce to the original unimodal van Genuchten–Mualem–type functions;

nc the non–capillary dominated flow domain;

w_c the weighting factor for capillary dominated flow domain c[–], subjected to $\Sigma\ w_c = 1$ and $0 < w_c < 1$.

When the soil is only bimodal (as shown by K-h measurements within the adopted tension range for our field site; Figure 3) and hence has only one capillary dominated and one non–capillary dominated flow domain, the hydraulic conductivity functions reduce to forms that closely resemble the Fermi function used by *Wilson et al.* [1992] and the bimodal function proposed by *Smettem and Kirkby* [1990]. However, the important difference between our approach and the Fermi function [*Wilson et al.*, 1992, equation 9] is that our K_0 is a floating parameter and depends on the (measured) K^* and (fitted) δ, while *Wilson et al.* [1992] fixed their K_s and K^* to match the observed K-θ data in the macropore region. In our study, as discussed earlier and unlike *Wilson et al.* [1992], we assumed that θ is partially mobile and gravity driven and that the change in θ near saturation may possibly be an (laboratory) experimental artifact, so that we could keep θ^* constant beyond h^* for our field soils. We also extrapolated K (in the tension range of less than h^*) from K^* using the nonlinear equation (4). In contrast, *Wilson et al.* [1992] adopted a linear interpolation technique between the two fixed points in their macropore region.

If no distinct changes in hydraulic conductivity were observed near saturation, we optimized our hydraulic parameters for the surface and subsurface horizons using the nonlinear optimization schemes of RETC (for steady state flow experiments [*van Genuchten et al.*, 1991]) and SFIT (for transient flow experiments [*Kool and Parker*, 1987]). For situations with bimodal hydraulic characteristics, the breakpoint soil water

Table 3. ⟨Field-Averaged⟩ Parameters of Bimodal Piecewise-Continuous and Unimodal van Genuchten–Mualem Hydraulic Functions for Different Soil Horizons at the Field Site in Las Nutrias, New Mexico

	Bimodal Piecewise-Continuous Hydraulic Functions						
Depth, cm	$\langle\theta_{\xi,t=1}\rangle$, $cm^3\ cm^{-3}$	$\langle\theta_{\xi,t=1}\rangle$, $cm^3\ cm^{-3}$	$\langle\alpha\rangle$, cm^{-1}	$\langle n\rangle$ (–)	$\langle K^*\rangle$, cm/s	$\langle h^*\rangle$, cm	$\langle\delta\rangle$, cm^{-1}
0–40	0.475	0.110	0.015	1.60	5.55E−04	3	0.92
40–100*	0.459	0.050	0.021	1.40	4.16E−04	3	0.70
100–700†	0.430	0.090	0.083	2.12	2.73E−03	0	n/a
	Unimodal van Genuchten-Mualem Hydraulic Functions (High/Low)						
Depth (cm)	$\langle\theta_s\rangle$, $cm^3\ cm^{-3}$	$\langle\theta_r\rangle$, $cm^3\ cm^{-3}$	$\langle\alpha\rangle$, cm^{-1}	$\langle n\rangle$ (–)	$\langle K_s\rangle$, cm/s		
0–40	0.484/0.475	0.080/0.120	0.004/0.015	1.44/1.55	4.08E−03/9.50E−04		
40–100	0.464/0.459	0.045/0.050	0.010/0.021	1.25/1.38	3.50E−03/6.80E−04		
100–700†	0.430/0.430	0.090/0.090	0.083/0.083	2.12/2.12	2.73E−03/2.73E−03		

The ⟨field-averaged⟩ parameters were obtained by fitting the van Genuchten–Mualem hydraulic functions (equations (1) and (3)) or the inverted exponential function (equation (4)) to (geometric or arithmetic) mean hydraulic data (e.g., as shown in Figures 4 and 5).

*As hydraulic parameters near saturation were not precise (using IP experiment) at deeper depths, $\langle h^*\rangle$, $\langle\delta\rangle$ parameters were adopted and calibrated from the surface horizon.

†As soil type varied from fine sand to sand in this depth range, flow was assumed to be well presented by unimodal van Genuchten–Mualem model.

pressure head (h^*) was determined by visual inspection, followed by separate nonlinear optimization of the hydraulic parameters for the capillary and noncapillary domains. Table 3 shows average values of the different hydraulic parameters optimized from field-averaged hydraulic functions (Figures 3 and 4) at different depths for our field site. Since the adopted IP experiment did not permit precise measurement of the subsurface hydraulic properties very close to saturation (as opposed to using the disc infiltrometer), we adjusted the hydraulic conductivity functions near saturation for the C1 (silty clay loam–silty clay) horizon by model calibration.

6. Numerical Modeling

The new hybrid sum-junction-type hydraulic functions were incorporated into the CHAIN_2D computer model [*Simunek and van Genuchten*, 1994] to enable two-dimensional transient flow simulations at the field site. We assumed that water flow, overall, could be described with Richards' equation (for Darcy-type flow under isothermal and variably saturated conditions) in conjunction with our bimodal (or multimodal) piecewise-continuous hydraulic functions. The soil was assumed to be rigid and nonhysteretic. For two-dimensional numerical simulations, the north-south cross section across the center bench was divided into 9350 nodes and 9126 quadrilateral elements (as shown in Figure 5) by subdividing the soil sampling and surface infiltration measurement grid (Figure 2). On the basis of the surface infiltration measurements and the IP experimental results, the soil profile was divided into three soil horizons (characterized by three ⟨field-averaged⟩ hydraulic functions). These three horizons were further subdivided into a total of 169 layers for numerical simulation purposes. Finer discretizations were used near the soil surface, across the horizon interfaces, and around the subsurface tile drain to handle intermittent (abrupt) changes in local fluxes and hence the pressure gradients. In addition, we kept our maximum vertical discretization relatively small ($\Delta z = 1$ cm) in the upper two horizons (of depth of 100 cm). Finer discretization improved the performance of numerical solutions, in particular when piecewise-continuous hydraulic functions were used in upper two horizons (i.e., $\Delta z < |h^*|$). For the simulations we used a time-variant evapotranspiration rate assuming a normalized water uptake distribution across the top 40 cm of the soil profile in accordance with the approach of *Feddes et al.* [1978]. Measured soil water contents before the crop growing season (i.e., February 1994 or 1995) at different nodal points and interpolated water table contours from the groundwater monitoring wells along the field boundary were used to define the initial conditions in the two-dimensional flow domain. Time-dependent boundary conditions, such as intermittent irrigation/precipitation rates at atmospheric boundary nodes; groundwater head values along hydrologic boundary nodes; and no-flow conditions along impermeable bottom boundary nodes were invoked. Since gradients of the groundwater table (Table 4) were found to be very small, we simplified the two hydrologic boundaries (Γ_{AD} and Γ_{BC}, Figure 5) by assuming impermeable boundaries. The tile drain at the center of the study section was treated as a boundary node surrounded by four regular square elements with adjusted hydraulic conductivities using the electric analog approach of *Vimoke et al.* [1963] and *Fipps et al.* [1986].

The initial value problem was solved assuming variably saturated flow [*Richards*, 1931], with the initial distribution of the pressure head within the flow domain, Ω, being a linear function of depth, and implementing system-independent, time-dependent specified fluxes including intermittent irrigation/rainfall and variable evapotranspiration rates (as shown in Figure 5). In addition to system-independent boundary conditions, CHAIN_2D considers system-dependent boundary conditions that cannot be defined a priori. For example, the potential fluid flux across the soil-air interface is controlled exclusively by external conditions (e.g., irrigation/rainfall). However, the actual flux depends also on the prevailing (transient) soil moisture conditions. Thus the soil surface boundary may change from prescribed flux to prescribed head-type conditions (and vice versa). The governing equation and associated initial and boundary conditions are hence as follows.

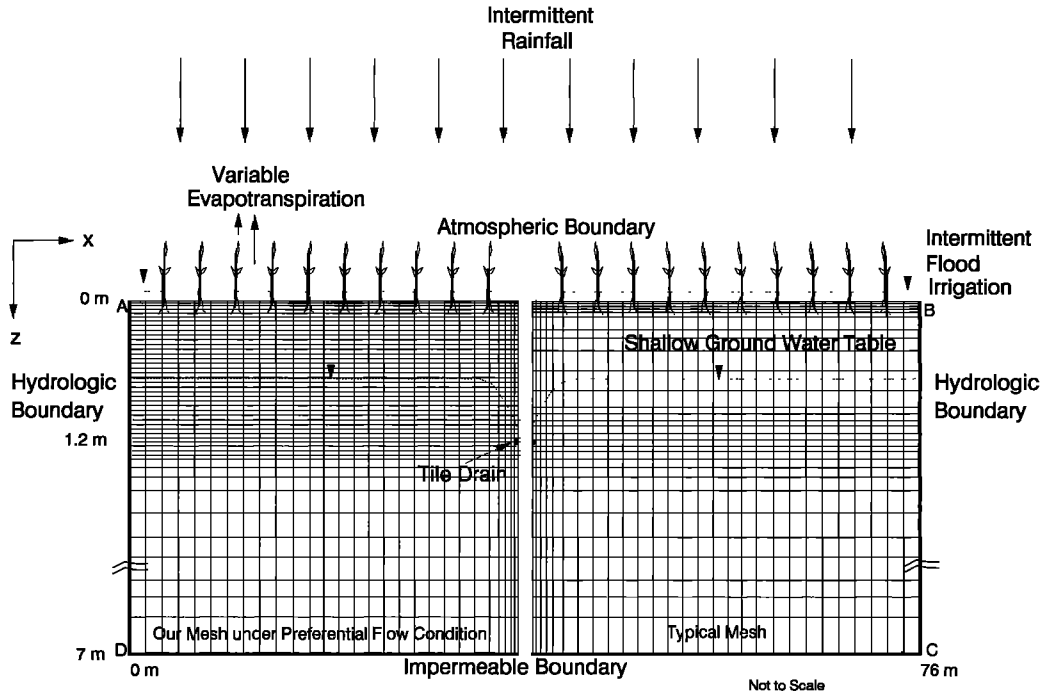

Figure 5. Typical/adapted finite element mesh including system-independent (time-dependent) and system-dependent flux/head-type atmospheric boundary, no-flux bottom and hydrologic boundaries, tile drain boundaries, and root water uptake sink term for the two-dimensional flow simulation in the vertical cross-section of the field (study section) at Las Nutrias, New Mexico. The cross section of unit length is assumed to be representative over the 240-m-long study section.

Governing Equation

$$\frac{\partial \theta}{\partial t} = \frac{\partial}{\partial x_i}\left[K\left(K_{ij}^A \frac{\partial h}{\partial x_j} + K_{iz}^A\right)\right] - S \tag{6}$$

where S is a sink term $[T^{-1}]$ for root water uptake, x_i $(i = 1, 2)$ are spatial coordinates $[L]$ (i.e., $x_1 = x$, and $x_2 = z$), t is time $[T]$, and K_{ij}^A are components of a dimensionless anisotropic conductivity tensor, K^A. Because no horizontal K measurements at deeper depths were made at the field site, we assumed K^A to be isotropic in this study. Other terms in (6) were defined before.

Initial Conditions

$$h(x, z, t) = h_0(x, z) \qquad t = 0 \in \Omega \tag{7}$$

where h_0 is a prescribed function of x and z in the flow region, Ω.

Boundary Conditions

System-Independent Atmospheric Boundary Γ_{AB}

$$-\left[K\left(K_{ij}^A \frac{\partial h}{\partial x_j} + K_{iz}^A\right)\right] n_i = \sigma_1(x, z, t) \tag{8}$$

$$(x, z) \in \Gamma_{AB} \qquad t \in t_{\text{flux}}$$

System-Dependent Atmospheric Boundary Γ_{AB}

$$\left|K\left(K_{ij}^A \frac{\partial h}{\partial x_j} + K_{iz}^A\right) n_i\right| \leq E \qquad (x, z) \in \Gamma_{AB} \tag{9}$$

and

$$h_A \leq h \leq h_s \qquad (x, z) \in \Gamma_{AB} \tag{10}$$

where σ[–] are prescribed (irrigation/rainfall water flux) functions of x, z, and t; and n_i are the components of the outward unit vector normal to the boundary Γ_{AB}; E is the maximum potential rate of infiltration or evaporation under the current atmospheric conditions; h is the pressure head at the soil surface; and h_A and h_s are, respectively, minimum and maximum pressure heads allowed under the prevailing soil conditions. When h_s was set to zero, E and h_A were calculated using relationships defined in *Feddes et al.* [1974].

Hydrologic Boundary Γ_{AD} and Γ_{BC} and Lower Impermeable Boundary Γ_{CD}

$$-\left[K\left(K_{ij}^A \frac{\partial h}{\partial x_j} + K_{iz}^A\right)\right] n_i = 0 \tag{11}$$

$$(x, z) \in \Gamma_{AD} \vee \Gamma_{BC} \vee \Gamma_{CD} \qquad \forall\, t$$

Tile Drain Boundary

$$K_{\text{drain}} = KC_d \tag{12}$$

where K_{drain} is the adjusted conductivity $[L\ T^{-1}]$ and C_d is a correction factor [–] to be calculated from the ratio of the effective drain diameter, d_e $[L]$, of the drain and the side length, D $[L]$, of the square formed by finite elements surrounding the drain node [*Vimoke and Taylor*, 1962].

Since this study focused on modeling preferential flow that would occur during or relatively soon after a large water input event (e.g., flood irrigation), we used hourly time steps and limited the real simulation time to approximately 100 hours from the start of an irrigation event. Also we adopted 0.1 hour (6 min) initial time steps for our numerical simulations to

closely follow the 5-min intervals of flow measurements in the field. For the numerical simulations we used a δ_θ convergence criterion [*Huang et al.*, 1996] in conjunction with the "mass conservative" modified Picard iteration method [*Celia et al.*, 1990] to enable relatively fast and robust convergence of the numerical solution. Other details of the numerical procedures adapted in CHAIN_2D are given by *Simunek and van Genuchten* [1994].

7. Simulation Results

Simulated tile flow using the new ⟨field-averaged⟩ bimodal piecewise-continuous soil water retention and hydraulic conductivity functions (Table 3) are presented in Figure 6 and compared against the field-observed values. We also compared the simulation results with results obtained using ⟨field-averaged⟩ unimodal van Genuchten–Mualem–type soil water retention and hydraulic conductivity functions. To present a qualitative comparison, we used two unimodal functions in the surface horizon based on $\langle K_{0\ mm}\rangle$ through $\langle K_{30\ mm}\rangle$ being included in the parameter optimization (unimodal_high), and $\langle K_{0\ mm}\rangle$ through $\langle K_{30\ mm}\rangle$ being excluded from the parameter optimization (unimodal_low). The short-term simulation runs were made separately by setting up the initial conditions and boundary conditions at the start of each simulation based on field measured data. Our simulations considered four flow scenarios: (1) the west bench irrigated prior to the center bench, (2) the center bench irrigated prior to the west bench, (3) irrigation during periods with a relatively low groundwater table (i.e., initially below the tile line), and (4) irrigation with a relatively high groundwater table (i.e., initially above the tile line). From the observed tile-drain flow it is clear, that following an irrigation event, water moves rapidly downward through the soil profile. Depending on initial conditions, and water input amount and intensity, different irrigation events required 10–20 hours for the water to reach the water table and subsequently the tile line. After a few hours of irrigation the tile flow rate suddenly increased and reached a peak that was almost instantly followed by a similar sharp drop, suggesting preferential flow through the field macropore network. This situation was followed by a recession phase dominated by prolonged matrix flow and water redistribution in the profile. In general, predicted flow using the bimodal hydraulic functions matched the observed flow rates reasonably well and far better than when the unimodal hydraulic functions were used.

A recent hypothetical study by *Zurmuhl and Durner* [1996] gave useful insight into the hydraulics of a similar type of bimodal porous medium. They found that transient soil water pressure head distributions versus depth changed far more abruptly for a bimodal soil than for a unimodal soil; our experimental and modeling results qualitatively agree with their findings. Our new hydraulic functions appear especially useful for flood-irrigation events when the water potential in the bulk soil can be represented more or less by a single value (as in unit gradient condition), unlike the multidomain or multiporosity approach. For this same reason the method may lose its advantage for lower-rate water application events. Furthermore, hysteretic, nonisothermal unsaturated flow, and three-dimensional groundwater flow are some of the missing characteristics of our modeling approach; these processes likely also contributed to the significant differences between observed and simulated flux values.

A comparison of the simulation results (Figure 6) for the four flow scenarios does reveal some interesting spatiotemporal phenomena governing tile flow in the experimental area. We emphasize here that no calibration of field-measured hydraulic functions was attempted during our field-scale-flow simulations. Peak flow predictions for scenario (1) slightly underestimated the observed peak. This is because west bench irrigation prior to the center bench irrigation reduced the groundwater table gradient in the east-west direction, thus forcing the subsurface flow field (with larger capture zone) to converge earlier to the tile drain. On the other hand, the higher east-west gradient in the groundwater table for scenario (2) caused a relatively delayed lower peak in the observed tile flow as compared to the model predictions. Furthermore, for scenario (3) tile flow showed atypical negative flow afterwards. We believe that this may have been an artifact of temporarily reversed flow from the downgradient (west) bench to the upgradient (center) bench; this could not be registered by the one-way tile-flow valve located in the west sump. A detailed discussion of some of these unusual flow processes near the manholes, and their governing factors, is given by B. P. Mohanty et al. (Preferential transport of nitrate to a tile drain in an intermittent-flood-irrigated field: Model development and experimental evaluation, submitted to *Water Resources Research*, 1997). Comparison of tile flow predictions for scenarios (3) and (4) shows better model performance under low groundwater table conditions at the field site. Although the exact reason for this behavior is still unknown, we believe that for the initially high groundwater table conditions, regional groundwater contribution to the tile flow may not have been properly accounted for using the adopted hydrologic boundary conditions in the two-dimensional model. A three-dimensional flow model may be a more suitable for our field site. We suspect also that temporal variability in the soil hydraulic prop-

Table 4. Mean Hydraulic Head and Hydraulic Gradients in Shallow Groundwater Aquifer Under the Center Bench Field in Las Nutrias, New Mexico

Date	Mean Head, m	Mean Gradient, m/m
	1994	
Feb.	98.79	4.30E−04
March	99.39	5.10E−04
April	99.24	1.00E−03
May	99.17	6.50E−04
June	99.20	7.20E−04
July	99.28	8.00E−04
Aug.	...	...
Sept.	99.17	6.30E−04
Oct.	98.95	8.00E−04
Nov.	98.90	7.20E−04
Dec.	98.85	7.20E−04
	1995	
Jan.	98.78	6.90E−04
Feb.	98.75	8.00E−04
March	98.95	5.80E−04
April	...	...
May	99.01	8.30E−04
June	99.10	8.70E−04
July	99.18	7.40E−04
Aug.	99.26	5.10E−04
Sept.	99.20	5.80E−04
Oct.	...	...

Ellipses denote no measurement. Reference elevation is 100.00 m at the soil surface.

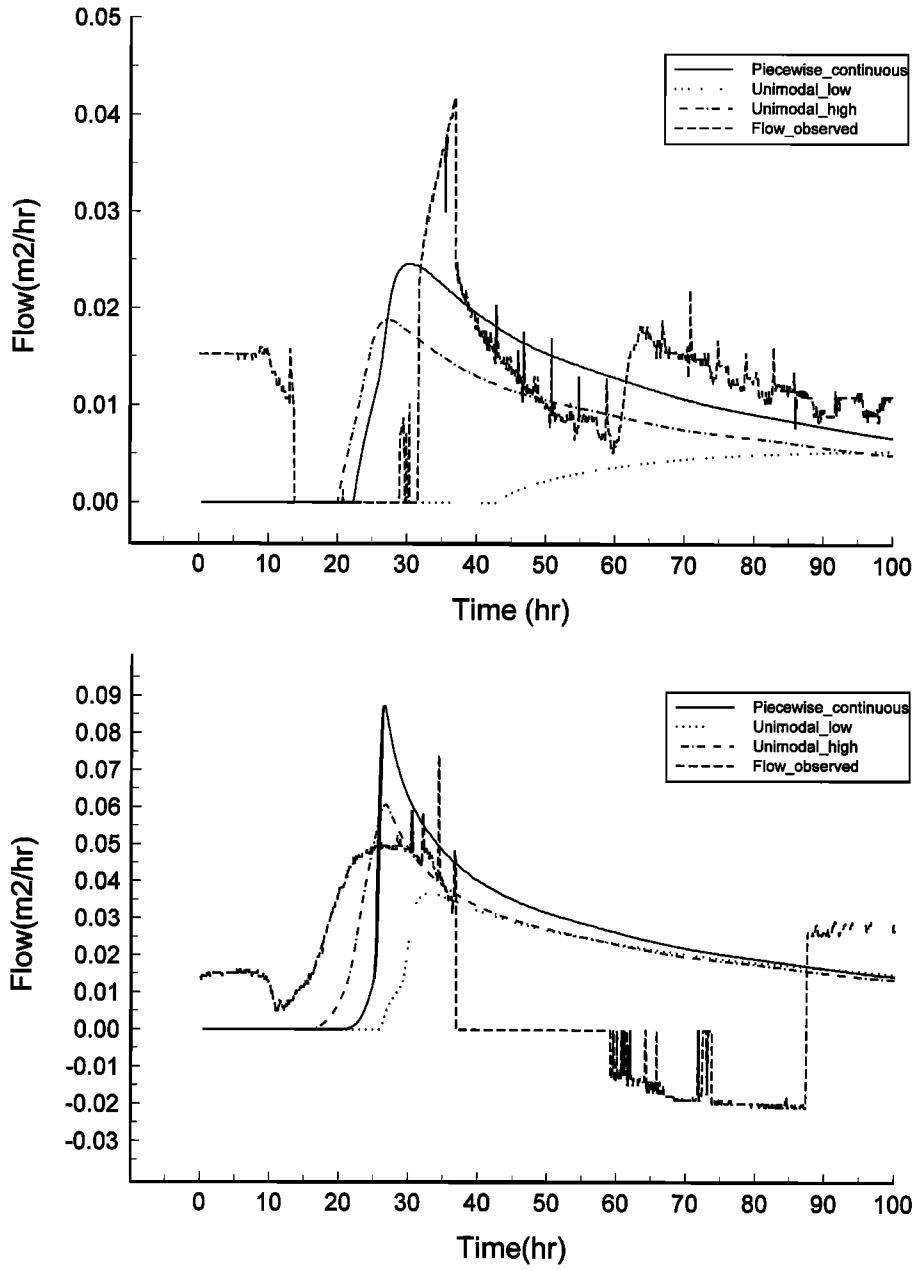

Figure 6. Comparison of simulated tile-drain flow (from the study section) using the piecewise-continuous hydraulic functions (bimodal soil porosity distribution) and the van Genuchten–Mualem (unimodal soil porosity distribution) hydraulic functions with observed data (net tile drain flow below the center bench) at the field site. (a) Scenario 1, west bench irrigated prior to the center bench; (b) scenario 2, center bench irrigated prior to west bench; (c) scenario 3, irrigation during (initially) low groundwater table condition; and (d) scenario 4, irrigation during (initially) high groundwater table condition. Time 0 corresponds to the midnight of the beginning day of center-bench irrigation.

erties may have played an important role in this behavior. A follow-up paper will address some of these issues, including spatial variability considerations using similar media scaling schemes.

Most importantly, from the different simulation runs we conclude that using the piecewise-continuous hydraulic functions generally minimized the overpredictions or underpredictions of flow in the different flow domains as is typically obtained with the one-domain approach. This study shows that matrix flow (during higher soil water tension) can be kept almost unchanged during calibration of the macropore flow domain (near saturation) and vice versa. We also found that the new piecewise-continuous hydraulic functions outperformed the unimodal function (unimodal_high with equal K_s) in terms of better predicting the timing and magnitude of the preferential flow peaks.

8. Concluding Remarks

Capillary flow–based unimodal soil water retention and hydraulic conductivity functions should be complemented with other functions to correctly simulate noncapillary dominated

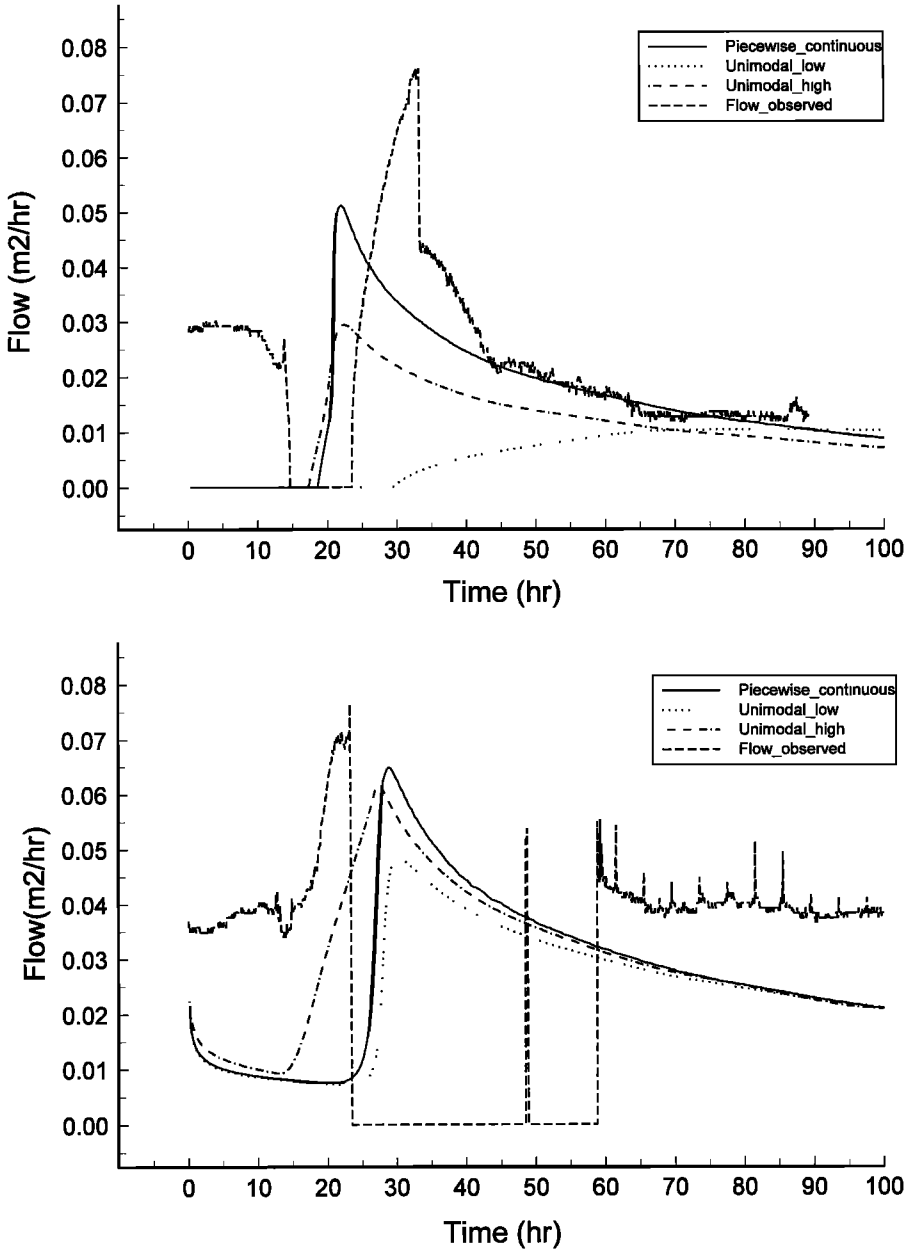

Figure 6. (continued)

flow near saturation in field soils. In this study we measured the relative trend of soil water retention and hydraulic conductivity functions near saturation and established piecewise-continuous functions to predict flow across a wide range of soil water tensions. The new hydraulic functions were used to predict the field-scale flow under a flood-irrigated field in Las Nutrias, New Mexico. A comparison of the performance of the new piecewise-continuous (bimodal) function with that of the (unimodal) van Genuchten–Mualem soil water retention and hydraulic conductivity functions showed that the new functions indeed performed better for the field soil. Unresolved issues of our new approach include (1) precision in differentiating the matching points (h^*, K^*, θ^*) for different types of soil, (2) precision of measurement of θ near saturation for different types of soil, and (3) description and inclusion of site-specific multidimensional regional hydrology in the mathematical model. To resolve some of these issues and to make the approach more robust, independent mathematical and more controlled (laboratory, field) experiments are warranted. Finally, our study also suggests that field-scale hydrologic model development always should be corroborated with field measurements.

Acknowledgments. This project was partly funded by the USDA-CSRS through special water quality grant 9301322. Thanks to graduate students Jeff Chaves, Tracy Roth, Bob Reedy, and Gunter Hilmes at New Mexico Institute of Mining and Technology, Socorro, New Mexico, for field and laboratory data collection.

References

Anderson, S. H., and J. W. Hopmans (Eds.), *Tomography of Soil Water Root Processes, Spec. Publ. 36*, Soil Sci. Soc. Am., Madison, Wis., 1994.

Andreini, M. S., and T. S. Steenhuis, Preferential paths of flow under conventional and conservation tillage, *Geoderma, 46*, 85–102, 1990.

Ankeny, M. D., Methods and theory for unsaturated infiltration measurements, in G. Topp et al. (editors), *Advances in Measurement of Soil Physical Properties: Bringing Theory into Practice, Spec. Publ. 30*, edited by G. Topp et al., pp. 123–141, Soil Sci. Soc. Am., Madison, Wis., 1992.

Ankeny, M. D., T. C. Kaspar, and R. Horton, Design of an automated tension infiltrometer, *Soil Sci. Soc. Am. J., 52*, 893–896, 1988.

Beven, K., and P. Germann, Macropores and water flow in soils, *Water Resour. Res., 18*, 1311–1325, 1982.

Booltink, H. W. G., Morphometric methods for simulation of water flow, Ph.D. thesis, Univ. of Wagennigen, Wagennigen, Netherlands, 1993.

Booltink, H. W. G., and J. Bouma, Sensitivity analysis on processes affecting bypass flow, *Hydrol. Processes, 7*, 33–43, 1993.

Booltink, H. W. G., J. Bouma, and D. Gimenez, A suction crust infiltrometer for measuring hydraulic conductivity of unsaturated soil near saturation, *Soil Sci. Soc. Am. J., 55*, 566–568, 1991.

Bouma, J., Soil morphology and preferential flow along macropores, *Agric. Water Manage., 3*, 235–250, 1981.

Bouma, J., and L. W. Dekker, A case study on infiltration into dry clay soil, I, Morphological observations, *Geoderma, 20*, 27–40, 1978.

Bowman, R. S., and R. C. Rice, Transport of conservative tracers in the field under intermittent flood irrigation, *Water Resour. Res., 22*, 1531–1536, 1986.

Campbell, G. S., and S. Shiozawa, Prediction of hydraulic properties of soils using particle-size distribution and bulk density data, in *Indirect Methods for Estimating the Hydraulic Properties of Unsaturated Soils*, edited by M. T. van Genuchten, F. J. Leij, and L. J. Lund, pp. 317–328, Univ. of Calif., Riverside, 1992.

Celia, M. A., E. T. Bouloutas, and R. L. Zabra, A general mass-conservative numerical solution for the unsaturated flow equation, *Water Resour. Res., 26*, 1483–1496, 1990.

Clothier, B. E., and K. R. J. Smettem, Combining laboratory and field measurements to define the hydraulic properties of soil, *Soil Sci. Soc. Am. J., 54*, 299–304, 1990.

Clothier, B. E., and I. White, Measurement of sorptivity and soil water diffusivity in the field soil, *Soil Sci. Soc. Am. J., 45*, 241–245, 1981.

Corey, A. T., Pore-size distribution, in *Indirect Methods for Estimatng the Hydraulic Properties of Unsaturated Soils*, edited by M. T. van Genuchten, F. J. Leij and L. J. Lund, pp. 37–44, Univ. of Calif., Riverside, 1992.

De Vries, J., and T. L. Chow, Hydrologic behavior of a forested mountain soil in coastal British Columbia. *Water Resour. Res., 14*, 935–942, 1978.

Durner, W., Hydraulic conductivity estimation for soils with heterogenous pore structure, *Water Resour. Res., 30*, 211–223, 1994.

Edwards, W. M., R. R. van der Ploeg, and W. Ehlers, A numerical study of the effects of non-capillary sized pores upon infiltration, *Soil Sci. Soc. Am. J., 43*, 851–856, 1979.

Edwards, W. M., L. D. Norton, and C. E. Remond, Characterizing macropores that affect infiltration into nontilled soil, *Soil Sci. Soc. Am. J., 52*, 483–487, 1988.

Ela, S. D., S. C. Gupta, and W. J. Rawls, Macropore and surface seal interactions affecting water infiltration into soil, *Soil Sci. Soc. Am. J., 56*, 714–721, 1992.

Everts, C. J., and R. S. Kanwar, Estimating preferential flow to a subsurface drain with tracers, *Trans. ASAE, 33*, 451–457, 1990.

Everts, C. J., and R. S. Kanwar, Interpreting tension-infiltrometer data for quantifying soil macropores: Some practical considerations, *Trans. ASAE, 36*, 423–428, 1993.

Feddes, R. A., E. Bresler, and S. P. Neuman, Field test of a modified numerical model for water uptake by root systems, *Water Resour. Res., 10*, 1199–1206, 1974.

Feddes, R. A., P. J. Kowalik, and H. Zaradny, *Simulation of Field Water Use and Crop Yield*, John Wiley, New York, 1978.

Fipps, G., R. W. Skaggs, and J. L. Nieber, Drains as a boundary condition in finite elements, *Water Resour. Res., 22*, 1613–1621, 1986.

Gardner, W. R., Calculation of capillary conductivity from pressure plate outflow data, *Soil Sci. Soc. Am. Proc., 20*, 317–320, 1956.

Gerke, H. H., and M. T. van Genuchten, A dual-porosity model for simulating the preferential movement of water and solutes in structured porous media, *Water Resour. Res., 29*, 305–319, 1993a.

Gerke, H. H., and M. T. van Genuchten, Evaluation of a first-order water transfer term of variably saturated dual-porosity flow models, *Water Resour. Res., 29*, 1225–1238, 1993b.

Germann, P. F., and K. Beven, Water flow in soil macropores, I, An experimental approach, *J. Soil Sci., 32*, 1–13, 1981.

Gwo, J. P., P. M. Jardine, G. V. Wilson, and G. T. Yeh, Using a multiregion model to study the effects of advective and diffusive mass transfer on local physical nonequilibrium and solute mobility in a structured soil, *Water Resour. Res., 32*, 561–570, 1996.

Hoogmoed, W. B., and J. Bouma, A simulation model for predicting infiltration into a cracked clay soil, *Soil Sci. Soc. Am. J., 44*, 458–461, 1980.

Huang, K., B. P. Mohanty, and M. T. van Genuchten, A new convergence criterion for the modified picard iteration method to solve the variably saturated flow equation, *J. Hydrol., 178*, 69–91, 1996.

Hutson, J. L., and R. J. Wagenet, A multiregion model describing water flow and solute transport in heterogenous soils, *Soil Sci. Soc. Am. J., 59*, 743–751, 1995.

Jardine, P. M., G. V. Wilson, R. J. Luxmoore, and J. F. McCarthy, Transport of inorganic and natural organic tracers through an isolated pedon in a forested watersheds, *Soil Sci. Soc. Am. J., 53*, 317–323, 1989.

Jardine, P. M., G. V. Wilson, and R. J. Luxmoore, Unsaturated solute transport through a forest soil during rain storm events, *Geoderma, 46*, 103–118, 1990.

Jarvis, N. J., and I. Messing, Near-saturated hydraulic conductivity in soils of contrasting texture measured by tension infiltrometers, *Soil Sci. Soc. Am. J., 59*, 27–34, 1995.

Klute, A., Water retention: Laboratory methods, in *Methods of Soil Analysis*, part I, *Agron. Monogr.*, vol. 9, edited by A. Klute, pp. 635–662, Am. Soc. of Agron., Madison, Wis., 1986.

Kool, J. B., and J. C. Parker, Estimating soil hydraulic properties from transient flow experiments: SFIT user's guide, Electr. Power Res. Inst., Palo Alto, Calif., 1987.

Logsdon, S. D., Flow mechanisms through continuous and buried macropores, *Soil Sci., 160*, 237–241, 1995.

Luckner, L., M. T. van Genuchten, and D. R. Nielsen, A consistent set of parametric models for the two-phase flow of immiscible fluids in the subsurface, *Water Resour. Res., 25*, 2187–2193, 1989.

Luxmoore, R. J., Micro-, meso-, and macro-porosity of soil, *Soil Sci. Soc. Am. J., 45*, 671, 1981.

Luxmoore, R. J., P. M. Jardine, G. V. Wilson, J. R. Jones, and L. W. Zelanzy, Physical and chemical controls of preferred path flow through a forested hill slope, *Geoderma, 46*, 139–154, 1990.

Mallants, D., D. J. Kim, J. Feyen, and P.-H. Tseng, Prediction of unsaturated hydraulic conductivity using multimodal hydraulic functions, *Eos Trans. AGU, 76*(46), Fall Meet. Suppl., F229, 1995.

Mapel, C. L., T. W. Sammis, and R. R. Lansford, Estimating crop water production functions based on transpiration and crop growth curves through modeling, *Rep. 191*, N. M. Water Resour. Res. Inst., Las Cruces, 1985.

Messing, I., and N. J. Jarvis, Temporal variation in the hydraulic conductivity of a tilled clay soils as measured by tension infiltrometers, *J. Soil Sci., 44*, 11–24, 1993.

Mohanty, B. P., M. D. Ankeny, R. Horton, and R. S. Kanwar, Spatial analysis of hydraulic conductivity measured using disc infiltrometers, *Water Resour. Res., 30*, 2489–2498, 1994.

Mohanty, B. P., R. Horton, and M. D. Ankeny, Infiltration and macroporosity under a row crop agricultural field in a glacial till soil, *Soil Sci., 161*, 205–213, 1996.

Natural Resource Conservation Service, Soil survey map of Las Nutrias, New Mexico, Lincoln, Nebr., 1992.

Othmer, H., B. Diekkruger, and M. Kutilek, Bimodal porosity and unsaturated hydraulic conductivity, *Soil Sci., 152*, 139–150, 1991.

Peters, R. R., and E. A. Klavetter, A continuum model for water movement in an unsaturated fractured rock mass, *Water Resour. Res., 24*, 416–430, 1988.

Phillips, R. E., V. L. Quisenberry, J. M. Zeleznik, and G. H. Dunn, Mechanism of water entry into simulated macropores, *Soil Sci. Soc. Am. J., 53*, 1629–1635, 1989.

Prieksat, M. A., M. D. Ankeny, and T. C. Kaspar, Design an automated, self-regulating, single-ring infiltrometer, *Soil Sci. Soc. Am. J., 56*, 1409–1411, 1992.

Richards, L. A., Capillary conduction of liquids in porous mediums, *Physics, 1*, 318–333, 1931.

Richards, L. A., Physical condition of water in soil, in *Methods of Soil*

Analysis, Part 1, *Agron. Monogr.*, vol. 9, edited by C. A. Black et al., pp. 128–152, Am. Soc. of Agron., Madison, Wis., 1965.

Rossi, C., and J. R. Nimmo, Modeling of soil water retention from saturation to oven dryness, *Water Resour. Res.*, *30*, 701–708, 1994.

Russo, D., Determining soil hydraulic properties by parameter estimation: On the selection of a model for the hydraulic properties, *Water Resour. Res.*, *24*, 453–459, 1988.

Samani, Z., Measuring water in trapezoidal canals, *J. Irrig. Drain. Eng.*, *119*, 181–186, 1993.

Seyfried, M. S., and P. S. C. Rao, Solute transport in undisturbed columns of an aggregated tropical soil: Preferential flow effects, *Soil Sci. Soc. Am. J.*, *51*, 1434–1444, 1987.

Simunek, J., and M. T. van Genuchten, The CHAIN_2D code for simulating the two-dimensional movement of water, heat, and multiple solutes in variably-saturated porous media, U.S. Salinity Lab., *Res. Rep. 136*, 1994.

Singh, P., R. S. Kanwar, and M. L. Thompson, Macropore characterization for two tillage systems using resin-impregnation technique, *Soil Sci. Soc. Am. J.*, *55*, 1674–1679, 1991a.

Singh, P., R. S. Kanwar, and M. L. Thompson, Measurement and characterization of macropores by using AUTOCAD and automatic image analysis, *J. Environ. Qual.*, *20*, 289–294, 1991b.

Smettem, K. R. J., and N. Collis-George, The influence of cylindrical macropores on steady-state infiltration in a soil under pasture, *J. Hydrol.*, *79*, 107–114, 1985.

Smettem, K. R. J., and C. Kirkby, Measuring the hydraulic properties of a stable aggregated soil, *J. Hydrol.*, *117*, 1–13, 1990.

van Genuchten, M. T., A closed-form equation for predicting the hydraulic conductivity of unsaturated soils, *Soil Sci. Soc. Am. J.*, *44*, 892–898, 1980.

van Genuchten, M. T., New issues and challenges in soil physics research, *Transactions of 15th World Congress of Soil Sci.*, vol. 1, 5–27; Int. Soc. of Soil Sci., Acapulco, Mexico, 1994.

van Genuchten, M. T., and D. R. Nielsen, On describing and predicting the hydraulic properties of unsaturated soils, *Ann. Geophys.*, *3*, 615–628, 1985.

van Genuchten, M. T., F. J. Leij, and S. R. Yates, The RETC code for quantifying the hydraulic functions of unsaturated soils, *EPA/600/2-91/065*, 85 pp., Environ. Prot. Agency, Ada, Okla., 1991.

Vimoke, B. S., and G. S. Taylor, Simulating water flow in soil with an electric resistance network, *Res. Rep. 41-65*, Soil and Water Conserv. Res. Div., USDA-ARS, Columbus, Ohio, 1962.

Vimoke, B. S., T. D. Tura, T. J. Thiel, and G. S. Taylor, Improvements in construction and of resistance networks for studying drainage problems, *Soil Sci. Soc. Am. Proc.*, *26*, 203–207, 1963.

Warner, G. S., J. L. Nieber, I. D. Moore, and R. A. Geise, Characterizing macropores in soil by computed tomography, *Soil Sci. Soc. Am. J.*, *53*, 653–660, 1989.

Watson, K. K., An instantaneous profile method for determining the hydraulic conductivity of unsaturated porous materials, *Water Resour. Res.*, *2*, 709–715, 1966.

Watson, K. W., and R. J. Luxmoore, Estimating macroporosity in a forest watershed by use of a tension infiltrometer, *Soil Sci. Soc. Am. J.*, *50*, 578–582, 1986.

White, R. E., The influence of macropores on the transport of dissolved and suspended matter through soil, in *Advances in Soil Science*, vol. 3, edited by B. A. Stewart, pp. 95–121, Springer-Verlag, New York, 1985.

Wilson, G. V., P. M. Jardine, and J. P. Gwo, Modeling the hydraulic properties of a multiregion soil, *Soil Sci. Soc. Am. J.*, *56*, 1731–1737, 1992.

Wilson, G. V., P. M. Jardine, R. J. Luxmoore, and J. R. Jones, Hydrology of a forested hillslope during storm events, *Geoderma*, *46*, 119–138, 1990.

Zurmuhl, T., and W. Durner, Modeling transient water and solute transport in a biporous soil, *Water Resour. Res.*, *32*, 819–829, 1996.

R. S. Bowman and J. M. H. Hendrickx, Department of Geoscience, New Mexico Institute of Mining and Technology, Socorro, NM 87801.

B. P. Mohanty and M. T. van Genuchten, U.S. Salinity Laboratory, 450 W. Big Springs Rd., Riverside, CA 92507. (e-mail: bmohanty@ussl.ars.usda.gov)

(Received October 4, 1996; revised May 10, 1997; accepted June 9, 1997.)